Cellular precipitates of iron oxide in olivine in a stratospheric interplanetary dust particle

FRANS J. M. RIETMEIJER

Department of Earth and Planetary Sciences, University of New Mexico, Albuquerque, NM 87131, USA

Abstract

The petrology of a massive olivine–sulphide interplanetary dust particle shows melting of Fe,Ni-sulphide plus complete loss of sulphur and subsequent quenching to a mixture of iron-oxides and Fe,Ni-metal. Oxidation of the fayalite component in olivine produced maghemite discs and cellular intergrowths with olivine and rare andradite-rich garnet. Cellular reactions require no long-range solid-state diffusion and are kinetically favourable during pyrometamorphic oxidation. Local melting of the cellular intergrowths resulted in three dimensional symplectic textures. Dynamic pyrometamorphism of this asteroidal particle occurred at ~1100°C during atmospheric entry flash (5–15 s) heating.

KEYWORDS: olivine, cellular precipitates, iron oxide, interplanetary dust.

Introduction

COLLISIONS with molecules in the Earth's atmosphere above 80–90 km altitude slow the orbital velocity of an interplanetary dust particle (IDP) from km s^{-1} to cm s^{-1} whereby it experiences a brief (5–15 s) period of heating. This ultrafast heating and cooling event (10^5–10^6°C/h) (Rietmeijer, 1996) may alter its pre-entry properties. The very nature of the flash-heating event is conducive to kinetically favourable mineral reactions. The maximum entry temperature of an individual IDP can be derived from its stepped heating He-release profile (Brownlee *et al.*, 1995) and used to obtain its entry velocity, and hence its probable origin (Love and Brownlee, 1991, 1994). This powerful method is fully appreciated but the chemistry, mineralogy and textures of heated IDPs have their own tale to tell. For example, these IDPs often show a characteristic (partial) rim of Fe-oxide that forms during atmospheric entry heating (Flynn, 1994) but this prominent mineralogical feature appears to be linked to the presence of sulphides. Other features due to atmospheric entry heating include laihunitisation of olivine (Keller *et al.*, 1992) and Fe,Ni-sulphide oxidation and vesiculation (Rietmeijer, 1993). Endothermic reactions, e.g. hydrocarbon pyrolysis (Bonny *et al.*, 1988) and sulphide decomposition below 525°C (Rietmeijer, 1992*a*), contribute to a thermal gradient in the particle during atmospheric entry. This gradient delays or prevents the particle interior from reaching the peak heating temperature (Flynn, 1995). As reaction kinetics depend on the nature of the time–temperature (T–t) regime, not every possible endothermic reaction will occur and it will be difficult to predict these mineral reactions in individual IDPs (Rietmeijer, 1992*b*). Oxidation reactions characterise terrestrial pyrometamorphic rocks that show Fe^{3+}-rich product phases, non-equilibrium mineral assemblages, incomplete mineral reactions, and partial fractional fusion at about 1000–1600°C (Foit, Jr. *et al.*, 1987; Cosca and Peacor, 1987; Cosca *et al.*, 1989). Pyrometamorphism in pelitic xenoliths in a Tertiary dolerite sill occurred at a time scale of 2–7 days between 750–900°C (Brearley, 1986, 1987*a*), while an experimental and kinetic study of the breakdown of aluminous biotite at 800°C indicated reaction times between 2 days and 8 weeks (Brearley, 1987*b*). Rietmeijer (1992*a*) proposed the term dynamic pyrometamorphism for mineral reactions that occurred in heated interplanetary dust particles during this unique short event of atmospheric entry. I present an analytical electron microscope [AEM] study of stratospheric IDP L2005U6 showing ablation and oxidation of the fayalite component in olivine due to dynamic pyrometamorphism of this particle. Its mineralogy shows that this heating event

Mineralogical Magazine, December 1996, Vol. 60, pp. 877–885

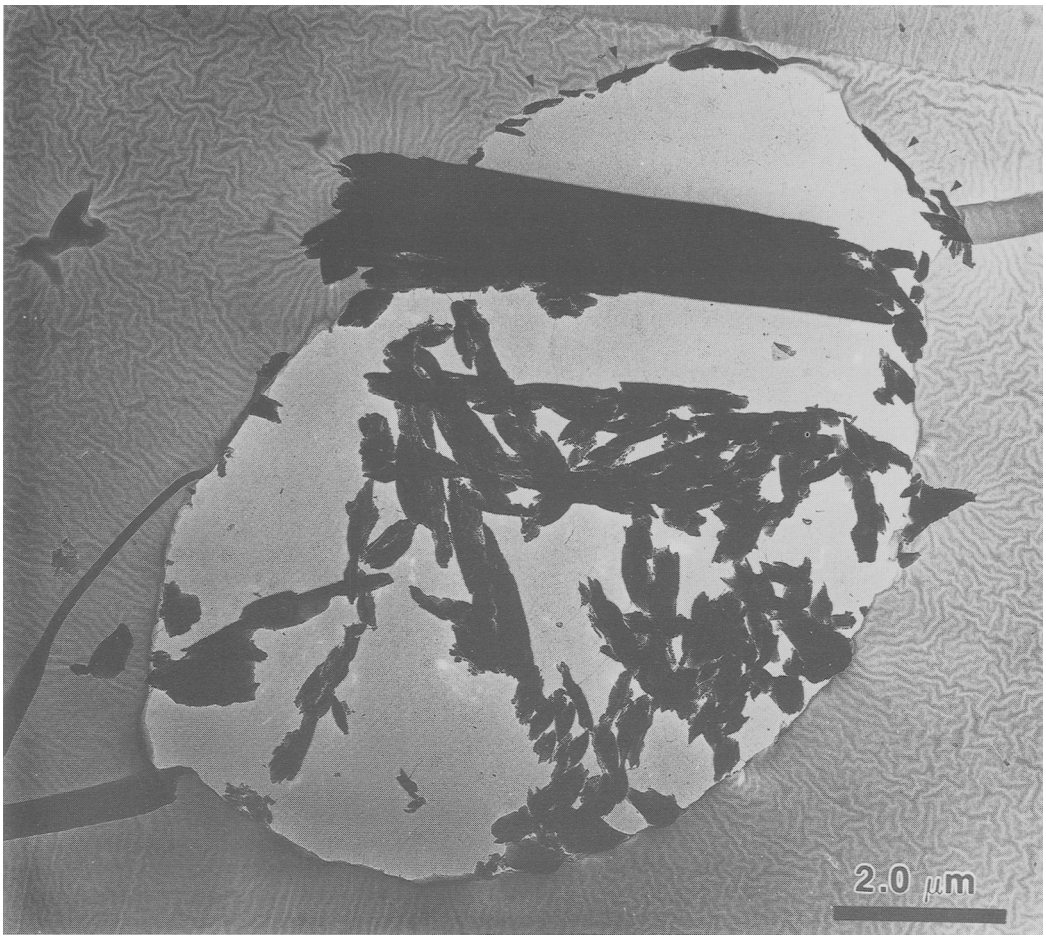

FIG. 1. Transmission electron photomicrograph showing substantial sample loss in an ultramicrotomed section of IDP L2005U6. The olivine part of this particle is below the electron opaque Fe,Ni-band that is a remnant of molten Fe,Ni-sulphides in the upper part of this IDP. Tiny arrows along the top show the maghemite rim on the sulphide part.

promoted cellular growth of maghemite but without the common coprecipitation of pyroxene(s).

Experimental

Particle L2005U6 was collected in the lower stratosphere during October 3–13, 1989, by the NASA Johnson Space Center (JSC) Cosmic Dust Program. It was embedded in epoxy at the NASA JSC Cosmic Dust Facility. Serial ultrathin sections (80–100 nm thick) were obtained in the Electron Microbean Analysis Facility at UNM where a JEOL 2000 FX AEM equipped with a Tracor-Northern TN5500 Energy Dispersive Spectrometer [EDS] was used for *in situ* thin-film analyses of elements with atomic number > 11. The Cliff and Lorimer (1975) thin-film correction procedure was used for quantitative analyses. The element k-factors for this procedure were established on mineral standards. The major oxide concentrations have a relative error < 5%. Crystallographical data were obtained by selected area electron diffraction [SAED] analyses. The SAED patterns were calibrated using a Au-coated holey carbon film that was analysed under similar conditions as the particle. Single-crystal SAED data have a relative error ~5%. The

TABLE 1. Comparison of interplanar spacings (nm) of the Fe,Ni-band in IDP L2005U6 with interplanar spacings for (1) magnetite (JCPDS file 19-629), (2) maghemite (JCPDS file 25-1402), (3) hematite (JCPDS file 33-664), (4) wüstite (JCPDS file 6-615), (5) kamacite (JCPDS file 18-645) and (6) taenite (JCPDS file 23-297)

Fe,Ni-phase	(1)	(2)	(3)	(4)	(5)	(6)
		2.505				
		0.791				
		0.694				
0.57		0.590				
0.55		0.533	0.503			
	0.485	0.482				
0.40		0.429		0.431	0.450	
		0.373				
0.36			0.368			0.360
0.34		0.340				
		0.320				
0.29	0.297	0.295			0.295	
0.28		0.278				
0.26	0.253	0.264	0.270			
0.24	0.242	0.241	0.252	0.249	0.246	
0.23		0.232	0.229		0.223	

interplanar spacings based on SAED 'ring' patterns for the Fe,Ni-rich phase have an error of ~10%, relative. Serial sections of the IDP from top to bottom allows a determination of its third dimension. The Fe-rich and olivine grains and dimensions of olivine–oxide intergrowths were measured directly on calibrated TEM photomicrographs. For each grain measurement a closest circle or ellipse was visually estimated to fit the grain. The measurements have a relative error of ~10%. Although most grains have a circular cross-section, the sizes are expressed as the root-mean-square size, r.m.s. = $\{a^2 + b^2\}^{1/2}$, where a and b are two orthogonal dimensions across the object.

Observations

The bean-shaped IDP L2005U6 measures 13 × 9.8 × 9.2 μm. The sections show considerable loss of material which is typical during ultramicrotomy of rapidly heated and quenched IDPs (Fig. 1). Both silicate and sulphide materials were lost but enough material remains to obtain reliable data on the particle interior. About 70% of the particle are silicates. The remainder is an Fe,Ni-phase. They have a distinct interface. A narrow (115 nm) maghemite rim is present on the Fe,Ni-phase along the particle surface. Isolated Fe,Ni-grains embedded in this rim contain a trace of sulphur with one grain up to Fe:Ni:S = 85:5:10 (at.%). This grain displays a vesicular texture. The Fe,Ni-rich phases are best preserved in a band adjacent to the silicate part. Dark field [DF] TEM imaging of this band using a strong diffraction maximum of the Fe,Ni phase reveals a mottled domain texture. Nickel contents in the band are in the range 10–27 at.% Ni. The combination of SAED (Table 1) and chemical data support the identification of iron-oxides, possibly maghemite (γ-Fe_2O_3), and Fe,Ni metal, probably taenite (γ-Fe,Ni) although the data can not exclude the presence of kamacite.

The silicate is single-crystal olivine (r.m.s size > 100 nm) plus garnet. DF TEM imaging of olivine, $Fo_{75}Fa_{23}La_2$ to $Fo_{52}Fa_{45.5}La_{2.5}$ (La is larnite, Ca_2SiO_4), shows a small scattered area with a mottled texture. All grains show lattice strain contrast associated with Fe-rich inclusions. The inclusions occur as discs and lamellar intergrowths with the host. The r.m.s. disc sizes are in the range 17–92 nm. Their lognormal size distribution reflects an under-abundance of small discs which is probably an artifact of the quality of ultrathin sections. About 20% of the discs have a noncircular cross-section with aspect ratios from 0.85 to 0.60 ($\mu = 0.75$). They typically show random dispersal but rare linear arrays parallel to $[001]_{oliv.}$ occur. The discs often show coalescence (Fig. 2*a*). Their 2.02 nm lattice fringes support maghemite.

The lamellar intergrowths of the Fe-rich phase and olivine are very regular (Fig. 2*b*). The ribbons are 27.8 nm wide (1σ = 8.4 nm; skewness = 0.6; N = 22) and spaced at 24.9 nm intervals (1σ = 7.0 nm; N = 19).

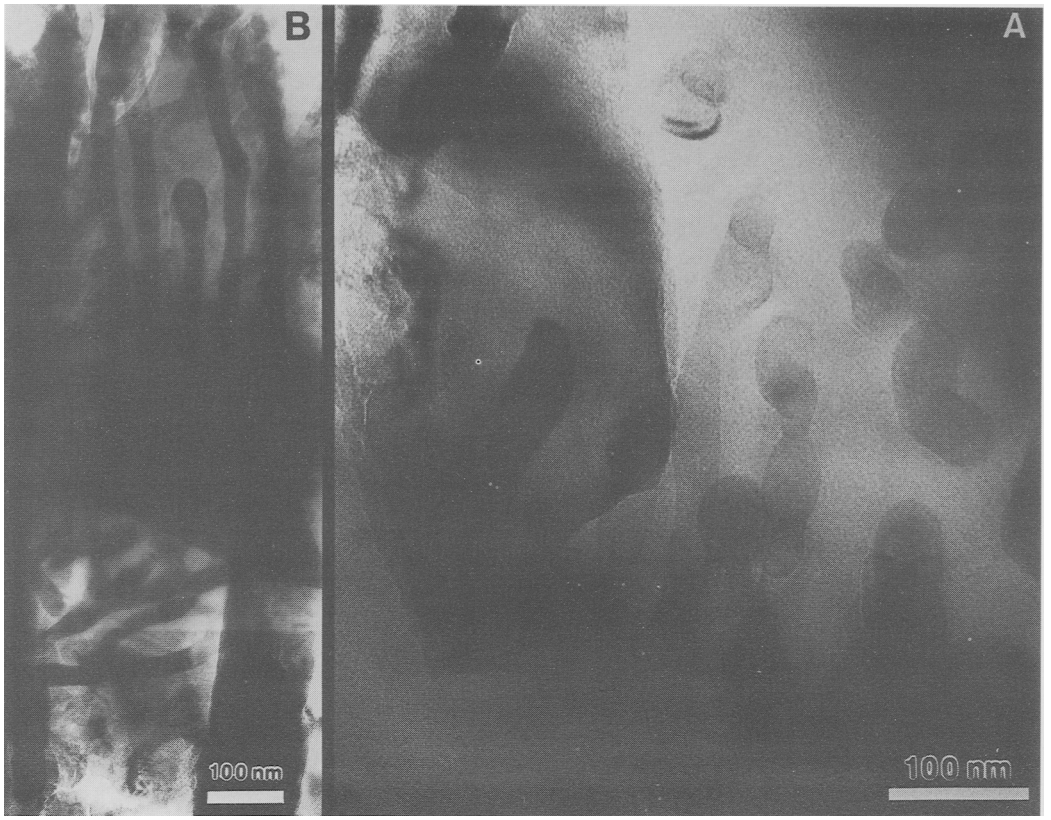

FIG. 2. (A) Transmission electron photomicrograph showing coagulation of iron oxide discs in olivine of IDP L2005U6. (B) *Ibid.*, a two-dimensional cellular intergrowth of maghemite and olivine.

Tilting the sample relative to the incident electron beam shows that the Fe-oxide lamellae are, in fact, thin ribbons. The single-crystal SAED data support tetragonal maghemite (Table 2). The basal plane of this oxide is almost parallel to the *bc*-plane of olivine. The lamellae are predominantly oriented // $[001]_{oliv}$ but also occur in the olivine *ac*-plane almost parallel to $[010]_{oliv}$. Similar maghemite ribbons occur in rare intergrowths with an andradite-rich garnet (Table 3) which reduces to $(Mg_{0.9}Fe^{2+}_{1.1}Ca_{1.2})(Fe^{3+}_{1.4}Al_{0.6})(Al_{0.3}Si_{2.7})O_{12}$. Weak diffraction maxima due to the garnet phase were observed in only one single-crystal SAED pattern of maghemite with a Burger's vector [001]. The garnet maxima were determined at 0.41, 0.32 and 0.19 nm. Comparison with X-ray data for $Mg_3Fe_2Si_3O_{12}$ (majorite) and $Ca_3Fe_2Si_3O_{12}$ (andradite) suggests that these maxima represent the garnet planes *hkl* 220 (0.407–0.426 nm, respectively), *hkl* 400 (0.288–0.3015 nm) and *hkl* 620 (0.182–0.191 nm).

Maghemite and olivine locally form three-dimensional vermicular intergrowths (Fig. 3). The scattered maghemite inclusions associated with these intergrowths are droplets rather than discs. Their sizes are comparable with the larger discs. Maghemite droplets, and rare subhedral platey maghemite grains (110–428.5 nm), are interspersed with rounded olivine grains. The r.m.s. sizes of Fe-oxide inclusions range from 284 to 855 nm with aspect ratios of 0.5–0.8 ($\mu = 0.7$). The smallest grains have a circular cross-section. Although the data are not entirely conclusive, an amorphous ferromagnesiosilica material seems to act as a cement for the olivine and maghemite grains in these restricted patches along the particle margin.

The density of randomly dispersed maghemite discs and droplets is highly variable. It is very difficult to obtain chemical analyses of inclusion-free olivine. With the exception of a few stoichiometric olivine structural formulae, i.e. the sum of cations (Σ)

TABLE 2. Comparison of interplanar spacings (nm) of iron oxides in IDP L2005U6 with interplanar spacings for maghemite (JCPDS file 25-1402), magnetite (JCPDS file 19-629), and hematite (JCPDS file 33-664)

Fe oxide	Maghemite	Magnetite	Hematite
2.02(*)	2.502		
	0.791		
	0.694		
	0.590		
	0.533		0.503
0.485	0.482	0.485	
	0.429		
0.38	0.373		0.368
	0.340		
0.32	0.320		
0.30	0.295	0.297	
	0.278		0.270
	0.264		
0.255		0.253	0.252
	0.241	0.242	
0.23	0.232		0.229

(*) lattice fringe spacing

TABLE 3. A representative analysis of garnet in IDP L2001U6

Wt.% of oxides		Number of cations in the formula based on 12 oxygens	
SiO_2	32.9	Si	2.74
Al_2O_3	8.3	Al	0.26
Fe_2O_3	23.0		
FeO	15.4	Al	0.55
MgO	7.3	Fe^{3+}	1.44
CaO	13.1		
		Fe^{2+}	1.07
		Mg	0.90
		Ca	1.17
		Σ	8.13

= 3.00 $\pm$ 0.03 (based on O = 4), the remainder invariably yield a structural formula with Si < 1.00 and Σ > 2.00. This general trend rather than the numbers supports the presence of ferric iron. The calculated ferric iron content in these olivines is < 6.8 el. wt.% Fe^{3+} (μ = 2.6 el. wt.% Fe^{3+}). The $Fe^{2+}/(Fe^{2+}+Fe^{3+})$ ratio is in the range 0.7–0.95 (μ = 0.87). The olivines typically contain < 1.7 el. wt.% Al (μ = 0.55 el. wt.%), and < 1.3 el. wt.% Ca (μ = 0.7 el. wt.%). Olivine compositions in the Mg-$Fe_{(total)}$-Si diagram are on a laihunite composition line. The bulk compositions (Fe > 45 el wt.%) for olivine with vermicular maghemite and droplets show a trend from laihunite-rich olivine to the Fe-apex (Fig. 4).

Pyrometamorphism

The morphology of extraterrestrial particle L2005U6 reflects surface melting and ablation during atmospheric entry heating. The co-occurrence of iron oxides and taenite is reminiscent of iron meteorite ablation debris (Blanchard and Davis, 1978) where these phases formed as a function of oxidation kinetics. The vesicular texture of a relic Fe,Ni-sulphide grain supports evaporative loss of sulphur (Rietmeijer, 1993), but in this particle heating resulted in Fe,Ni-sulphide melting with complete loss of sulphur. The original micrometeoroid was probably a grain of Fe,Ni-sulphide attached to a Mg,Fe-olivine grain. This particular combination of major elements is common to debris of micrometeoroids captured in near-Earth space by impact onto spacecraft and satellite surfaces (Brownlee *et al.*, 1974; Laurance and Brownlee, 1986; Rietmeijer *et al.*, 1986; Zolensky *et al.*, 1994). Olivines and Fe,Ni-sulphides were identified in debris from impact features on the Solar Maximum satellite (Rietmeijer and Blanford, 1988) and Long Duration Exposure Facility (Zolensky *et al.*, 1994).

Oxidation of olivine occurs in meteorite fusion crusts (Brownlee *et al.*, 1975) whereby the phenomena associated with olivine were well established by artificial meteor ablation studies (Blanchard and Cunningham, 1974). The resulting olivine-magnetite symplectites invariably show an associated silica phase (Blanchard and Cunningham, 1974). The general nature of the assemblage silica plus magnetite, or hematite, and the role of oxidation as the rate-controlling step, were established by oxidation experiments on fayalite under controlled gas phase compositions (Mackwell, 1992). Heating experiments (in air) of Mg,Fe-olivines of different composition showed that the silica phase due to symplectite formation is metastable in the presence of forsterite with a $MgSiO_3$ phase forming after prolonged heating at 1100°C (Champness, 1970). The duration of these heating experiments ranged from 8 days at 650°C to 3 days between 800°C and 1200°C (Champness, 1970). These symplectic intergrowths with coprecipitated silica and $MgSiO_3$, or Ca-rich clinopyroxene (Moseley, 1984), occur in many lunar and terrestrial olivines. Most investigators invoked oxidation of olivine but Moseley (1984) proposed a model of exsolution whereby Fe^{3+} for magnetite growth was already present in the Mg,Fe-olivine structure as a hypothetical component

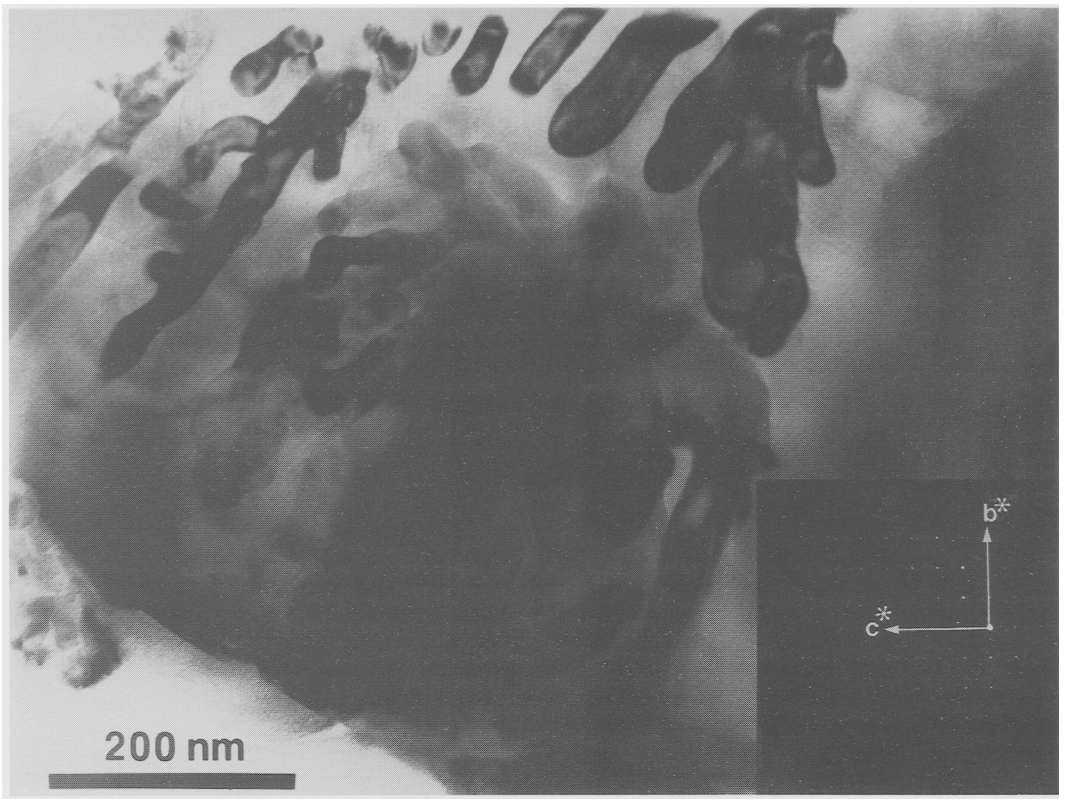

FIG. 3. Transmission electron photomicrograph of a maghemite-olivine symplectite in IDP L2005U6 (*cf.*, upper-right portion of the image). Tilting experiments reveal the three dimensional symplectite nature. The inset is an SAED pattern for the olivine host.

$Fe^{3+}_{4/3}SiO_4$. This component reacted with fayalite to magnetite plus silica, $Fe^{3+}_{4/3}SiO_4 + Fe^{2+}_2SiO_4 = 2Fe^{3+}_2Fe^{2+}O_4 + 4SiO_2$ (Moseley, 1984).

The product phases rewritten as $Fe^{2+}Fe^{3+}_2Si_2O_8$ are identical to the stoichiometric laihunite formula (Kitamura *et al.*, 1984). Kondoh *et al.* (1985) later established that laihunite is a nonstoichiometric distorted olivine-type mineral. It formed by oxidation of fayalite and is often associated with magnetite and silica. The mottled laihunite texture reported by Kitamura *et al.* (1984) is comparable to this texture of olivine in L2005U6.

The regular thickness and spacing of maghemite ribbons in olivines in this particle indicate a cellular decomposition reaction. Cellular reactions allow rapid growth of the precipitate by eliminating the necessity for long-range diffusion. It is possible that in L2005U6 a laihunite component in its olivine decomposed into γ-Fe_2O_3 plus Mg,Fe-olivine. For the discussion, I use the formula for nonstoichiometric laihunite (Kondoh *et al.*, 1985), *viz.* $\square_x Fe^{2+}_{2-3x}Fe^{3+}_{2x}SiO_4$ where I adopt $x = 0.1$.

This choice will not affect the general nature of the reaction,

$$\square_{0.1}Fe^{2+}_{1.7}Fe^{3+}_{0.2}SiO_4 + 0.3\ MgO = Mg_{0.3}Fe_{1.7}SiO_4 + 0.1\gamma\text{-}Fe_2O_3 \quad (1)$$

Adjacent Mg,Fe-olivines will contribute MgO for this reaction and cause small-scale compositional adjustment. Rare Fe^{3+}-rich garnet formed by reaction of more oxidised laihunite (e.g. $x = 0.6$) and Mg,Fe-olivine, *viz.*

$$\square_{0.6}Fe^{2+}_{0.2}Fe^{3+}_{1.2}SiO_4 + 2\ Mg_{1.5}Fe_{0.5}SiO_4 = Mg_3Fe^{3+}_2Si_3O_{12} \quad (2)$$

For simplicity the reactions are written without Ca and Al. Both elements and ferric iron were incorporated in this nesosilicate which is structurally similar to olivine rather than in a chain silicate. Natural terrestrial pyrometamorphic reac-

tions and those that yielded cellular precipitates in olivine heating experiments occur on time scales of several days which compares with only a few seconds for mineral reactions in interplanetary dust entering the Earth's atmosphere. While clinopyroxenes in terrestrial pyrometamorphic rocks incorporate high amounts of ferric iron (Cosca and Peacor, 1987), clinohypersthene in these rocks does not (Hensen and Gray, 1979). It seems plausible that low Ca content of IDP L2005U6 kinetically favoured the formation of Fe^{3+}-rich garnet. This particle is the first occurrence of garnet in interplanetary dust.

Lattice misfit across the olivine-oxide interface is < 5% with additional lattice strain due to precipitate maturation (Champness, 1970), differential thermal expansion of olivine and maghemite, or both. Lattice strain is much less evident in the symplectites. The compositions of the intergrowths of these three dimensional precipitates and olivine (Fig. 4) were recalculated for presentation in the MgO–FeO–Fe_2O_3–SiO_2 liquidus phase diagram (f_{O_2} for air) (Muan and Osborn, 1956). They are clustered on the olivine–magnesioferrite cotectic line at 1600°C. Magnesioferrite was not observed in L2005U6 but Champness (1970) noted that iron oxides in these intergrowths may contain magnesium. This cluster of bulk compositions on the cotectic line suggests that local melting was established at appropriate olivine/Fe-oxide ratios.

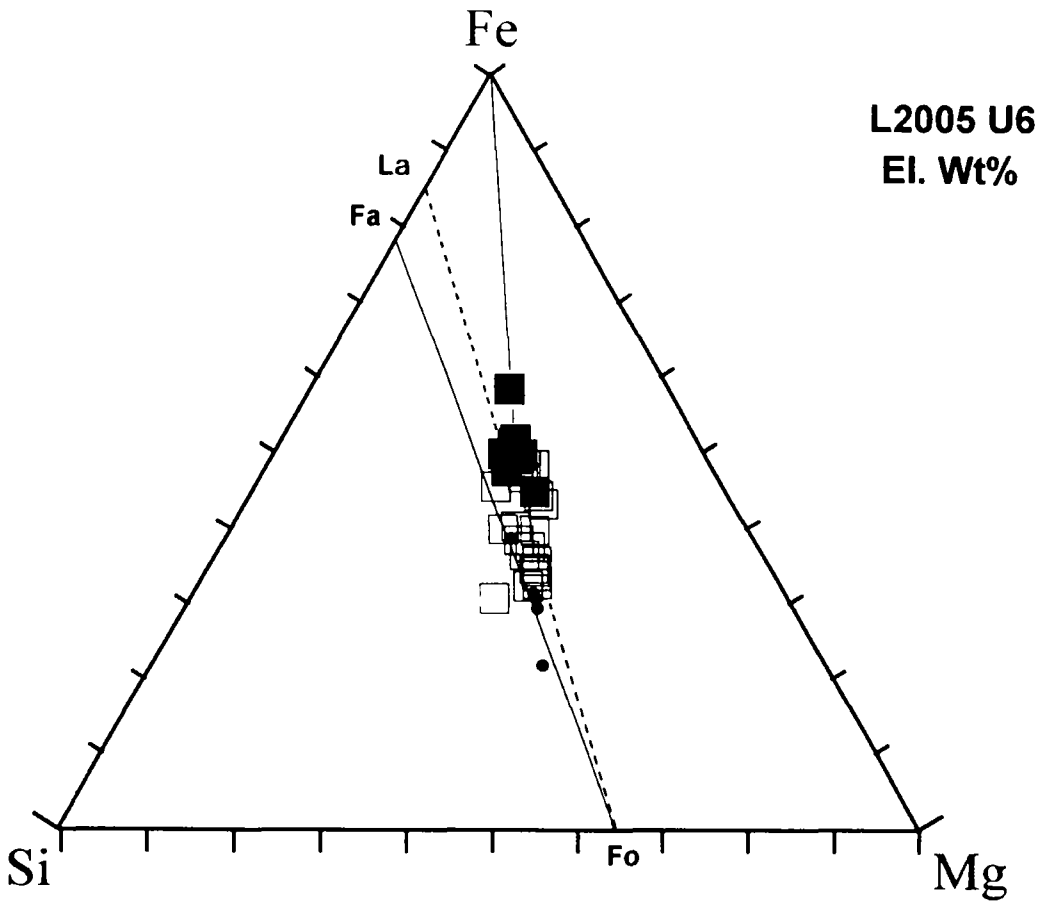

FIG. 4. Olivine compositions in IDP L2005U6 in a ternary diagram Mg-Fe-Si (el. wt%). Open squares are for olivine with dispersed maghemite precipitates. Solid squares indicate the bulk compositions (Fe > 45 el. wt.%) of the maghemite-olivine symplectite. The dashed line delineates the laihunite component in Mg,Fe-olivines. The dots are olivine debris in impact feature M-19-280 on the Solar Maximum satellite surface (Rietmeijer and Blanford, 1988).

Particle thermometry and origin

Models of *T-t* profiles in IDPs during atmospheric entry are sufficiently sophisticated that in combination with internal thermometers it is possible to separate asteroidal from cometary dust on the basis of atmospheric entry velocity. Due to uncertainties in the velocity determinations the results are occasionally inconclusive and other arguments must be brought forward to make the distinction. The petrological properties of some IDPs are sufficiently unique of a probable origin and they may serve to test the models. That is, an origin derived from a match of peak heating temperature and particle size and mass, and hence entry velocity, must be consistent with particle petrology.

Equilibrium melting of olivines in this IDP occurs at 1550–1600°C but it probably started at lower temperatures as pressures in the atmosphere above 80 km altitude are $<10^{-6}$ bar. Under these conditions olivine melting mimics the Mg,Fe-olivine solid-gas relations at ~1100°C (Nagahara *et al.*, 1991). The cotectic temperature at 1600°C for the three dimensional intergrowths is probably an upper limit as strain in the olivine lattice may contribute to lowering the melting point. Olivine oxidation experiments showed that spacings of oxide needles in cellular reactions were 5–15 nm after eight days at 500–950°C and 200 nm after three days at 1050°C (Champness, 1970). These experiments also indicated that time is not a limiting factor above 1050°C. It appears that the cellular reaction in L2005U6 occurred below 950°C but in this IDP the kinetically favoured cellular reaction may have occurred at higher temperatures to mimic the long-duration experiments. In summary, the peak heating temperature of L2005U6 was probably close to 1100°C.

Love and Brownlee (1991) presented a diagram of entry velocity as a function of peak heating temperature for a particle with a density of 2 g/cm^3. Since the product of particle diameter and density is constant, their diagram can be used to obtain the entry velocity of any IDP of known density and diameter from its peak heating temperature. The effective diameter (D_a= (a+b+c)/3) of L2005U6 is 10.7 μm and it's estimated density is 4 g/cm^3 [$(0.7\times3.7)_{ol.}$ + $(0.3\times4.8)_{sulph.}$ g/cm^3]. Hence, its peak heating temperature of 1100°C indicates an atmospheric entry velocity of 15.5 km/s at an average entry angle of 45° (*cf.* Love and Brownlee, 1994). The lowest possible temperature in this particle (950°C) yields an entry velocity of 13 km/s. A steeper entry angle increases the peak heating temperature and results in a lower velocity. This situation is reversed for more grazing atmospheric incidence. These velocities support an origin in the asteroid belt which is consistent with mineralogy and grain sizes in this particle.

Conclusions

The formation of maghemite and andradite-rich garnet to accommodate Ca, Al and Fe^{3+}, as well as surface melting in IDP L2005U6 were kinetically favourable reactions in the uniquely short (5–15 s) *T-t* regime of dynamic pyrometamorphism on atmospheric entry of this particle. Garnets in IDPs are probably unique indicator minerals of atmospheric entry flash heating. In this massive olivine-sulphide particle the resulting cellular reaction for maghemite precipitation in olivine required no long-range solid-state diffusion. The sulphide phase melted with complete loss of sulphur. Its melt quenched into a mixture of an iron oxide (probably maghemite) and Fe,Ni-metal. The petrology of this particle supports peak heating to ~1100°C which yields a particle velocity of 13–15.5 km/s consistent with an asteroidal origin. This work showed that it is possible to constrain IDP origins based dynamic pyrometamorphic mineralogies.

Acknowledgements

I greatly appreciate a careful review by Monica Grady. I thank Stan Love for evaluations of the atmospheric entry temperatures derived in this paper. John Bradley made suggestions that improved this paper. The AEM analyses were performed at the Electron Microbean Analysis Facility in the Department of Earth and Planetary Sciences at UNM where Fleur Rietmeijer-Engelsman provided technical assistance. This work was supported by the National Aeronautics and Space Administration, grant NAGW-3626.

References

Blanchard, M.B. and Cunningham, G.C. (1974) Artificial meteor ablation studies: Olivine. *J. Geophys. Res.*, **79**, 3973–90.

Blanchard, M.B. and Davis, A.S. (1978) Analysis of ablation debris from natural and artificial iron meteorites. *J. Geophys. Res.*, **83(B4)**, 1793–808.

Bonny, Ph., Balageas, D., Devezeaux, D. and Maurette, M. (1988) Atmospheric entry of micrometeorites containing organic materials (abstract). *Lunar Planet. Sci.*, **19**, 118–9.

Brearley, A.J. (1986) An electron optical study of muscovite breakdown in pelitic xenoliths during pyrometamorphism. *Mineral. Mag.*, **50**, 385–97.

Brearley, A.J. (1987*a*) A natural example of the disequilibrium breakdown of biotite at high temperature: TEM observations and comparison with experimental kinetic data. *Mineral. Mag.*, **51**, 93–106.

Brearley, A.J. (1987*b*) An experimental and kinetic

study of the breakdown of aluminous biotite at 800°C: reaction microstructures and mineral chemistry. *Bull. Mineral.*, **110**, 513–32.

Brownlee, D.E., Tomandl, D.A., Hodge, P.W. and Horz, F. (1974) Elemental abundances in interplanetary dust. *Nature*, **252**, 667–9.

Brownlee, D.E., Blanchard, M.B., Cunningham, G.C., Beauchamp, R.H. and Fruland, R. (1975) Criteria for identification of ablation debris from primitive meteoric bodies. *J. Geophys. Res.*, **80**, 4917–24.

Brownlee, D.E., Joswiak, D.J., Schlutter, D.J., Pepin, R.O., Bradley, J.P. and Love, S.G. (1995) Identification of individual cometary IDP's by thermally stepped He release (abstract). *Lunar Planet. Sci.*, **26**, 183–4.

Champness, P.E. (1970) Nucleation and growth of iron oxides in olivine $(Mg,Fe)_2SiO_4$. *Mineral. Mag.*, **37**, 790–800.

Cliff, G. and Lorimer, G.W. (1975) The quantitative analysis of thin specimens. *J. Microscopy*, **103**, 203–7.

Cosca, M.A. and Peacor, D.R. (1987) Chemistry and structure of essenite ($CaFe^{3+}AlSiO_6$), a new pyroxene produced by pyrometamorphism. *Amer. Mineral.*, **72**, 148–57.

Cosca, M.A., Essene, E.J., Geissman, J.W., Simmons, W.B. and Coates, D.A (1989) Pyrometamorphic rocks associated with naturally burned coal beds, Powder River Basin, Wyoming. *Amer. Mineral.*, **74**, 85–100.

Flynn, G.J. (1994) Changes to the composition and mineralogy of interplanetary dust particles by terrestrial encounters. In *Analysis of Interplanetary Dust* (M.E. Zolensky, T.L. Wilson, F.J.M. Rietmeijer and G.J. Flynn, eds), pp. 127–44. Amer. Inst. Phys. Conf. Proc. 310. Amer. Inst. Phys. Press, New York,

Flynn, G.J. (1995) Thermal gradients in interplanetary dust particles: The effect of an endothermic phase transition (abstract). *Lunar Planet. Sci.*, **26**, 405–6.

Foit, Jr., F.F., Hooper, R.L. and Rosenberg, P.E. (1987) An unusual pyroxene, melilite, and iron oxide mineral assemblage in a coal-fire buchite from Buffalo, Wyoming. *Amer. Mineral.*, **72**, 137–47.

Hensen, B.J. and Gray, D.R. (1979) Clinohypersthene and hypersthene from a coal fire buchite near Ravensworth, N.S.W., Australia. *Amer. Mineral.*, **64**, 131–5.

Keller, L.P., Thomas, K.L. and McKay, D.S. (1992) Thermal processing of cosmic dust: Atmospheric entry heating and parent body metamorphism (abstract). *Lunar Planet. Sci.*, **23**, 675–6.

Kitamura, M., Shen, B., Banno, S. and Morimoto, N. (1984) Fine textures of laihunite, a nonstoichiometric distorted olivine-type mineral. *Amer. Mineral.*, **69**, 154–60.

Kondoh, S., Kitamura, M. and Morimoto, N. (1985) Synthetic laihunite ($\square_x Fe^{2+}_{2-3x}Fe^{3+}_{2x}SiO_4$), an oxidation product of olivine. *Amer. Mineral.*, **70**, 737–746.

Laurance, M.R. and Brownlee, D.E. (1986) The flux of meteoroids and orbital space debris striking satellites in low Earth orbit. *Nature*, **323**, 136–8.

Love, S.G. and Brownlee, D.E. (1991) Heating and thermal transformation of micrometeoroids entering the Earth's atmosphere. *Icarus*, **89**, 26–43.

Love, S.G. and Brownlee, D.E. (1994) Peak atmospheric entry temperatures of micrometeorites. *Meteoritics*, **29**, 69–70.

Mackwell, S.J. (1992) Oxidation kinetics of fayalite (Fe_2SiO_4). *Phys. Chem. Minerals*, **19**, 222–8.

Moseley, D. (1984) Symplectic exsolution in olivine. *Amer. Mineral.*, **69**, 139–53.

Muan. A. and Osborn, E.F. (1956) Phase equilibria at liquidus temperatures in the system MgO–FeO–Fe_2O_3–SiO_2. *J. Amer. Ceram. Soc.*, **39**, 121–40.

Nagahara, H., Kushiro, I. and Mysen, B.O. (1991) The system Mg_2SiO_4–Fe_2SiO_4 at low pressure. In *Ann. Rpt. Dir. Carnegie Inst. Wash. 1990–1991*, pp. 88–92. Carnegie Inst. Washington.

Rietmeijer, F.J.M. (1992*a*) Endothermic reactions constrain dynamic pyrometamorphic temperatures in two iron-rich interplanetary dust particles (abstract). *Lunar Planet. Sci.* , **23**, 1151–2.

Rietmeijer, F.J.M. (1992*b*) Pregraphitic and poorly graphitised carbons in porous chondritic micrometeorites. *Geochim. Cosmochim. Acta*, **56**, 1665–71.

Rietmeijer, F.J.M. (1993) Micrometeorite dynamic pyrometamorphism: Observation of a thermal gradient in iron-nickel sulfide (abstract). *Lunar Planet. Sci.*, **24**, 1201–2.

Rietmeijer, F.J.M. (1996) The ultrafine mineralogy of a molten interplanetary dust particle as an example of the quench regime of atmospheric entry heating. *Meteoritics Planet. Sci.*, **31**, 237–42.

Rietmeijer, F.J.M. and Blanford, G.E. (1988) Capture of an olivine micrometeoroid by spacecraft in low-Earth orbit. *J. Geophys. Res.*, **93(B10)**, 11,943–8.

Rietmeijer, F.J.M., Schramm, L.S., Barrett, R.A., McKay, D.S. and Zook, H.A. (1986) The main electronics box thermal blanket of the Solar Maximum satellite as an inadvertent capture cell for orbital debris and micrometeors. *Adv. Space Sci.*, **6**, 145–9.

Zolensky, M.E., Hörz, F., See, T., Bernhard, R., Dardano, C., Barrett, R.A., Mack, K. and Warren, J. (1994) Meteoroid investigations using the Long Duration Exposure Facility. In *Analysis of Interplanetary Dust* (M.E. Zolensky, T.L. Wilson, F.J.M. Rietmeijer and G.J. Flynn, eds.), pp. 291–304. Amer. Inst. Phys. Conf. Proc. 310. Amer. Inst. Phys. Press, New York.

[Manuscript received 19 January 1996: revised 10 April 1996]